

A 2-D meshless model for jointed rock structures

Xiong Zhang^{1,*†}, Mingwan Lu¹ and J. L. Wegner²

¹ *Department of Engineering Mechanics, Tsinghua University, Beijing 100084, People's Republic of China*

² *Department of Mechanical Engineering, University of Victoria, Victoria, B.C., Canada V8N 3P6*

SUMMARY

According to the characteristic structural features of jointed rock structures, a meshless model is proposed for the mechanics analysis of jointed rock structures based on the moving least-squares interpolants. In this model, a jointed rock structure is regarded as a system of relatively intact rock blocks connected by joints or planes of discontinuity; these rock blocks are modelled by general shaped anisotropic blocks while these joints and planes of discontinuity are modelled by interfaces. The displacement field of each block is constructed by the moving least-squares interpolants with an array of points distributed in the block. To deal with the discontinuities of rock structures, the displacement fields are constructed to be discontinuous between blocks. The displacement fields and their gradients are continuous in each block, hence no post processing is required for the output of strains and stresses. The finite element mesh is totally unnecessary, so the time-consuming mesh generation is avoided. The rate of convergence can exceed that of finite elements significantly, and a high resolution of localized steep gradients can be achieved. Furthermore, the discontinuities of rock structures are also fully taken into consideration. The present method is developed for two-dimensional linear elastic analysis of jointed rock structures, and can be extended to three-dimensional and non-linear analysis. Copyright © 2000 John Wiley & Sons, Ltd.

KEY WORDS: block-interface model; meshless method; element-free Galerkin method; rock mechanics

1. INTRODUCTION

Because of the presence of joints and planes of discontinuity, the behaviour of jointed rock structures is largely controlled by the discontinuities. A rock structure can be regarded as a system of relatively intact rock blocks connected by joints or planes of discontinuity. Many numerical methods have been proposed, such as Joint Element [1], Discrete Element Method [2], Discontinuous Deformation Analysis [3], Rigid Finite Element Method [4], Block-Interface Model [5], and several others. All these methods require discretization of rock masses into a great number of

*Correspondence to: Xiong Zhang, Department of Engineering Mechanics, Tsinghua University, Beijing 100084, People's Republic of China

†E-mail: xzhang@263.net

Contract/grant sponsor: National Natural Science Foundation of China; Contract/grant number: 59509002

finite elements to achieve reasonable results, consequently, mesh generation for these methods is a time-consuming task.

Besides the time-consuming mesh generation, mesh-based methods are also not well suited to the problems associated with extremely large deformations of the mesh and problems associated with frequent remeshing. Although several strategies have been developed to maintain a reasonable mesh shape, such as the Arbitrary Lagrangian–Eulerian (ALE) method [6], extra computational effort and difficulties are also introduced. In the simulation of failure processes, frequent remeshing is required to model the propagation of cracks with arbitrary and complex paths so that the computational effort required is very significant.

Compared with the finite element method, meshless methods have overcome these difficulties, and some of them have a number of attractive features. Many researchers were interested in meshless methods, and about 10 different meshless methods have been developed, such as the Element-Free Galerkin (EFG) method [7], the Reducing Kernel Particle Method (RKPM) [8], the Smoothed Particle (SPH) method [9], and several others. The journal, *Computational Methods in Applied Mechanics and Engineering*, published a special issue on meshless methods in December, 1996. In these methods, EFG constructs its shape functions by the moving least-squares (MLS) interpolants.

In the Block-Interface Model proposed in Reference [5], a rock structure is discretized by blocks, which are in a constant stress state, connected by interfaces. The blocks are used to model the rock blocks while the interfaces are used to model the joints and planes of discontinuity. For a rock block with steep stress gradient, it should be further divided into many sub-blocks. Consequently, the preparation of data is a time-consuming task, and the continuity condition between these sub-blocks must be imposed by penalty method. Based on paper [5], a meshless model is proposed by introducing MLS into the Block-Interfaces Model to construct the displacement fields of the blocks without dividing them into sub-blocks. According to the characteristic structural features of rock structures, a rock structure is regarded as a system of relatively intact anisotropic rock blocks connected by interfaces, and every rock block is modelled by an array of points through the moving least-squares interpolants (see Figure 1). To reduce the computational effort required for a large-scale rock structure, the major part of the structure, in which stress gradients are moderately low, can be modelled by a few large anisotropic blocks whose material properties can be obtained from an equivalent anisotropic continuum model [10–13]. It is unnecessary to divide each block into sub-blocks, so that the time-consuming mesh generation is avoided. The displacement fields and their gradients are continuous in each block, hence no post processing is required for the output of strains and stresses. Furthermore, the discontinuities of rock structures are fully taken into consideration in the present method.

2. DEFORMATION OF BLOCKS

The displacement $u(\mathbf{x})$ at point \mathbf{x} is approximated locally by the moving least-squares interpolants as

$$u^h(\mathbf{x}) = \sum_{j=1}^m p_j(\mathbf{x}) a_j(\mathbf{x}) \equiv \mathbf{p}^T(\mathbf{x}) \mathbf{a}(\mathbf{x}) \quad (1)$$

where coefficients $a_j(\mathbf{x})$ are functions of \mathbf{x} , $p_1(\mathbf{x}) = 1$ and $p_j(\mathbf{x})$ are monomials in the space coordinates $\mathbf{x} = [x, y]^T$ so that the basis is complete. A linear basis in a two-dimensional domain

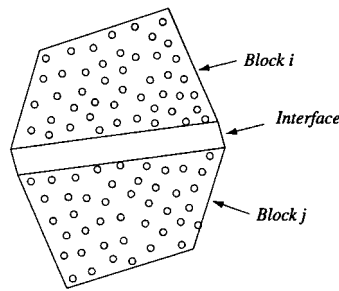


Figure 1. Block-interface model based on the moving least-squares interpolants.

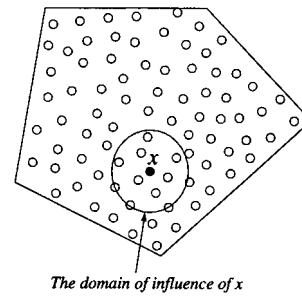


Figure 2. The domain of influence of \mathbf{x} .

provided by

$$\mathbf{p}^T(\mathbf{x}) = [1, x, y], \quad m = 3 \tag{2}$$

and a quadratic basis by

$$\mathbf{p}^T(\mathbf{x}) = [1, x, y, x^2, xy, y^2], \quad m = 6 \tag{3}$$

In the finite element method, if linear basis is used, the shape function of a triangle element can be obtained by letting the nodal value of the local approximation $u^h(\mathbf{x})$ at point x_I , $u^h(\mathbf{x}_I)$, equal that of the function $u(\mathbf{x})$ at the point x_I , u_I . The derivatives of the shape functions of this kind of methods are discontinuous between elements. In the moving least-squares interpolants, coefficients $a_j(\mathbf{x})$ are obtained at point \mathbf{x} by minimizing

$$J = \sum_I^n w(\mathbf{x} - \mathbf{x}_I) [\mathbf{p}^T(\mathbf{x}_I) \mathbf{a}(\mathbf{x}) - u_I]^2 \tag{4}$$

where n is the number of points in the neighbourhood of \mathbf{x} for which the weight function $w(\mathbf{x} - \mathbf{x}_I) \neq 0$. This neighborhood of \mathbf{x} is called the domain of influence of \mathbf{x} , or circle of influence in two dimensions (see Figure 2). The domain of influence of a point never extends across any boundaries, thus the domain of influence of the point \mathbf{x} is limited to those points \mathbf{x}_I which are located in the same block as the point \mathbf{x} . For computational efficiency, the weight function $w(\mathbf{x} - \mathbf{x}_I)$ should be compactly supported, that is to say, the influence domain of \mathbf{x} should be relatively small.

The stationarity of J in (4) with respect to $\mathbf{a}(\mathbf{x})$ leads to

$$\mathbf{A}(\mathbf{x}) \mathbf{a}(\mathbf{x}) = \mathbf{B}(\mathbf{x}) \mathbf{u}_a \tag{5}$$

where

$$\mathbf{A}(\mathbf{x}) = \sum_{I=1}^n w_I(\mathbf{x}) \mathbf{p}(\mathbf{x}_I) \mathbf{p}(\mathbf{x}_I)^T \tag{6}$$

$$\mathbf{B}(\mathbf{x}) = [w_1(\mathbf{x}) \mathbf{p}(\mathbf{x}_1), w_2(\mathbf{x}) \mathbf{p}(\mathbf{x}_2), \dots, w_n(\mathbf{x}) \mathbf{p}(\mathbf{x}_n)] \tag{7}$$

$$\mathbf{u}_a^T = [u_1, u_2, \dots, u_n], \tag{8}$$

$$w_I(\mathbf{x}) \equiv w(\mathbf{x} - \mathbf{x}_I) \tag{9}$$

Solving (5) for $\mathbf{a}(\mathbf{x})$ and then substituting $\mathbf{a}(\mathbf{x})$ into (1), we have

$$u^h(\mathbf{x}) = \Phi(\mathbf{x})\mathbf{u}_a \quad (10)$$

where the shape function $\Phi(\mathbf{x})$ is defined by

$$\Phi(\mathbf{x}) = \mathbf{p}^T(\mathbf{x})\mathbf{A}^{-1}(\mathbf{x})\mathbf{B}(\mathbf{x}) \quad (11)$$

The interpolation function $u^h(\mathbf{x})$ obtained from (10) is a local approximation of the function $u(\mathbf{x})$ at point \mathbf{x} , and it is calculated by the interpolation of the nodal values of the function $u(\mathbf{x})$ at those points distributed in the domain of influence of \mathbf{x} . The interpolation function $u^h(\mathbf{x})$ is a patch function, hence the global stiffness matrix is a sparse matrix.

The function $u^h(\mathbf{x})$ needs to be calculated at every quadrature point for assembly of the global stiffness matrix and load vector, consequently, equation (5) also needs to be solved at every quadrature point. If $\mathbf{p}(\mathbf{x})$ is an orthogonal basis, the matrix $\mathbf{A}(\mathbf{x})$ will be a diagonal matrix so that (5) can be solved easily. However, the computational effort required for the orthogonalization of $\mathbf{p}(\mathbf{x})$ is almost equal to that required for solving (5) directly. In this paper, the basis given in (2) and (3) are used.

In the finite element method, the coefficient matrix $\mathbf{a}(\mathbf{x})$ in (1) is a constant matrix within each element, but it is not the case with the moving least-squares interpolants. The partial derivatives of the shape function $\Phi(\mathbf{x})$ can be obtained as follows:

$$\Phi_{,i}(\mathbf{x}) = \mathbf{p}_{,i}^T(\mathbf{x})\mathbf{A}^{-1}(\mathbf{x})\mathbf{B}(\mathbf{x}) + \mathbf{p}^T(\mathbf{x})\mathbf{A}^{-1}(\mathbf{x})[\mathbf{B}_{,i}(\mathbf{x}) - \mathbf{A}_{,i}(\mathbf{x})\mathbf{A}^{-1}(\mathbf{x})\mathbf{B}(\mathbf{x})] \quad (12)$$

The weight functions $w_I(\mathbf{x})$ play an important role in the present method. They should be constructed so that they are positive and that a unique solution of $\mathbf{a}(\mathbf{x})$ is guaranteed; they should be relatively large for the \mathbf{x}_I close to \mathbf{x} , and relatively small for the more distant \mathbf{x}_I . The weight function,

$$w_I(d_I) = \begin{cases} \frac{e^{-(d_I/c)^2} - e^{-(d_{ml}/c)^2}}{1 - e^{-(d_{ml}/c)^2}} & \text{if } d_I \leq d_{ml} \\ 0 & \text{if } d_I > d_{ml} \end{cases} \quad (13)$$

proposed in [7] is used in this paper. In (13), c is a constant which determines the shape of the weight functions, $d_I = \|\mathbf{x} - \mathbf{x}_I\|$ is the distance between the two points \mathbf{x} and \mathbf{x}_I , d_{ml} is the size of the support for the weight function $w_I(d_I)$ and determines the domain of influence of x . Figure 3 shows the weight functions for $d_{ml}/c = 2, 5$ and 8 . In this paper, d_{ml}/c is selected as $2 \leq d_{ml}/c \leq 8$.

If the size of the domain of influence of \mathbf{x} , d_{ml} , is too small, the matrix $\mathbf{A}(\mathbf{x})$ will be singular. However, very large domains of influence result in a global stiffness matrix with large band widths, so that the computational effort required is increased significantly. The choice of d_{ml} should guarantee that the total number of points located in the domain of influence of \mathbf{x} , n , is not less than the order of the basis, m , and these n points are not in a straight line.

For a two-dimensional problem, the displacement vector, $\mathbf{u} = [u, v]^T$, at point \mathbf{x} in a block can be obtained from (10) as

$$\mathbf{u} = \mathbf{N}\mathbf{u}_b \quad (14)$$

where

$$\mathbf{N} = \begin{bmatrix} \Phi_1(\mathbf{x}) & 0 & \Phi_2(\mathbf{x}) & 0 & \cdots & \Phi_n(\mathbf{x}) & 0 \\ 0 & \Phi_1(\mathbf{x}) & 0 & \Phi_2(\mathbf{x}) & \cdots & 0 & \Phi_n(\mathbf{x}) \end{bmatrix} \quad (15)$$

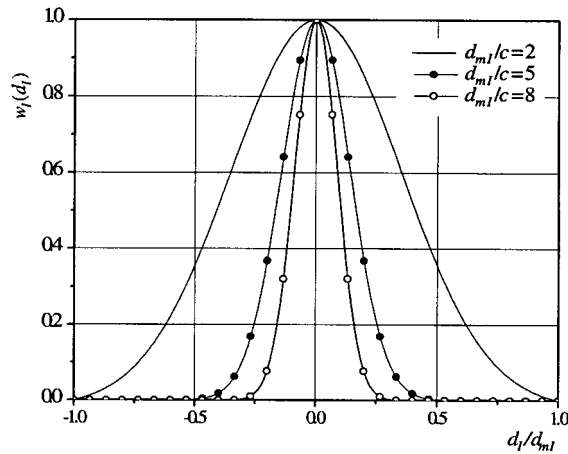


Figure 3. The weight functions $w_l(d_l)$ for different values of d_{mf}/c .

$$\mathbf{u}_b = [u_1, v_1, u_2, v_2, \dots, u_n, v_n]^T \tag{16}$$

The strain ε and stress σ at point \mathbf{x} in a block are given by

$$\varepsilon = \mathbf{B}_b \mathbf{u}_b \tag{17}$$

$$\sigma = \mathbf{D}_b \mathbf{B}_b \mathbf{u}_b \tag{18}$$

where \mathbf{D}_b is the elasticity matrix of the block,

$$\mathbf{B}_b = \begin{bmatrix} \Phi_{1,x} & 0 & \Phi_{2,x} & 0 & \dots & \Phi_{n,x} & 0 \\ 0 & \Phi_{1,y} & 0 & \Phi_{2,y} & \dots & 0 & \Phi_{n,y} \\ \Phi_{1,y} & \Phi_{1,x} & \Phi_{2,y} & \Phi_{2,x} & \dots & \Phi_{n,y} & \Phi_{n,x} \end{bmatrix} \tag{19}$$

$$\varepsilon = [\varepsilon_x, \varepsilon_y, \gamma_{xy}]^T, \quad \sigma = [\sigma_x, \sigma_y, \tau_{xy}]^T \tag{20}$$

3. DEFORMATION OF INTERFACES

Consider the deformation at point P in the interface shown in Fig. 4. Generally speaking, the width h of an interface is much less than its length L , hence the strain in the n direction in the interface can be assumed to be constant. The relative deformation vector δ at point P in the interface between its top and bottom surfaces is given by

$$\delta = [\delta_n, \delta_s] = \bar{\mathbf{u}}_j - \bar{\mathbf{u}}_i \tag{21}$$

where δ_n and δ_s are the normal and shear relative deformation at point P in the interface between its top and bottom surfaces, respectively, $\bar{\mathbf{u}}_i$ and $\bar{\mathbf{u}}_j$ are the displacement vectors in the local co-ordinate system n - s at points i and j , respectively. They are related to the displacement vectors \mathbf{u}_i and \mathbf{u}_j in the global coordinate system x - y by

$$\bar{\mathbf{u}} = \mathbf{L} \mathbf{u} \tag{22}$$

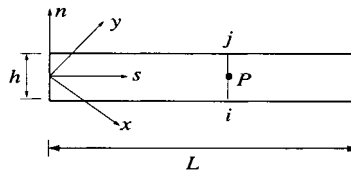


Figure 4. A interface.

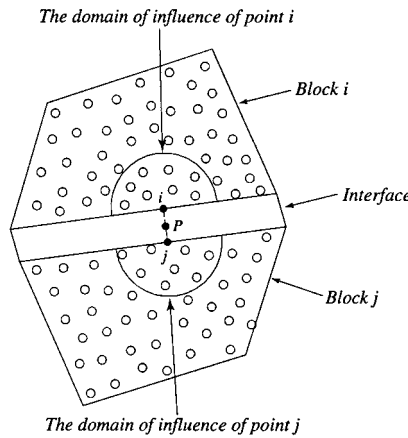


Figure 5. The domain of influence of points *i* and *j*.

where **L** is the co-ordinate transform matrix composed of the direction cosines of vectors *n* and *s*. Introducing (14) and (22) into (21) leads to

$$\delta = \mathbf{B}_s \mathbf{u}_s \tag{23}$$

where

$$\mathbf{B}_s = [-\mathbf{LN}_i, \mathbf{LN}_j] \tag{24}$$

$$\mathbf{u}_s = [\mathbf{u}_{bi}^T, \mathbf{u}_{bj}^T]^T \tag{25}$$

\mathbf{u}_{bi} and \mathbf{u}_{bj} are the displacement vectors composed of displacement at all points in the domains of influence of points *i* and *j*, respectively. Note that points are only distributed within each rock block, and no points are put in interface zone. The domain of influence of points *i* and *j* are limited within block *i* and *j*, respectively, and cannot be extended to the interface zone (see Figure 5). Consequently, the displacement vector \mathbf{u}_s in (25) is composed of displacement of points distributed within the domain of influence of points *i* and *j*.

Compared with other strain components, the normal strain component in the *s* direction can be neglected, hence the strain vector in the local co-ordinate system *n-s* at point *P* in the interface can be defined as

$$\varepsilon' = \frac{1}{h} \delta \tag{26}$$

where $\varepsilon' = [\varepsilon_n, \gamma_{ns}]^T$, ε_n is the normal strain in the *n* direction, and γ_{ns} is the shear strain.

The normal stress in the s direction also can be neglected compared with other stress components. The stress vector \mathbf{R} composed of the normal stress σ_n and the tangential shear stress τ_s in the interface is related to the relative deformation vector δ by

$$\mathbf{R} = \mathbf{D}_s \delta \tag{27}$$

where

$$\mathbf{D}_s = \frac{1}{h} \begin{bmatrix} \frac{E}{1-\nu^2} & 0 \\ 0 & \frac{E}{2(1+\nu)} \end{bmatrix} \text{ for plane strain problems} \tag{28}$$

$$\mathbf{R} = [\sigma_n, \tau_s]^T \tag{29}$$

The matrix \mathbf{D}_s can also be defined by the normal stiffness coefficient K_n and the tangential shear stiffness coefficient K_s of the interface as

$$\mathbf{D}_s = \begin{bmatrix} K_n & 0 \\ 0 & K_s \end{bmatrix} \tag{30}$$

4. VARIATIONAL PRINCIPLE

The modified variational principles for discontinuous mediums, such as rock structures, was established in [14] and [5]. The static equilibrium equations of a rock structure can be obtained from these variational principles. The functional of the overall potential energy of a rock structure is given by

$$\Pi^* = \Pi_e + \Pi_s + \Pi_f + \Pi_p \tag{31}$$

where Π_e and Π_s are the elastic strain energy of blocks and interfaces, respectively, Π_f and Π_p are the potential energy of the surface force \mathbf{f}_e and the concentrated force \mathbf{p}_m applied in blocks, respectively. They are given by

$$\Pi_e = \sum_e t_e \iint_{\Omega_e} \frac{1}{2} \boldsymbol{\varepsilon}^T \mathbf{D}_b \boldsymbol{\varepsilon} \, dx \, dy = \frac{1}{2} \sum_e \mathbf{u}_b^T \left(t_e \iint_{\Omega_e} \mathbf{B}_b^T \mathbf{D}_b \mathbf{B}_b \, dx \, dy \right) \mathbf{u}_b \tag{32}$$

$$\Pi_s = \sum_k t_k \int_{\beta_k} \frac{1}{2} \delta^T \mathbf{D}_s \delta \, ds = \frac{1}{2} \sum_k \mathbf{u}_s^T \left(t_k \int_{\beta_k} \mathbf{B}_s^T \mathbf{D}_s \mathbf{B}_s \, ds \right) \mathbf{u}_s \tag{33}$$

$$\Pi_f = - \sum_e \iint_{\Omega_e} \mathbf{u}^T \mathbf{f}_e \, dx \, dy = - \sum_e \mathbf{u}_b^T \left(\iint_{\Omega_e} \mathbf{N}^T \mathbf{f}_e \, dx \, dy \right) \tag{34}$$

$$\Pi_p = - \sum_m \mathbf{u}^T \mathbf{p}_m = - \sum_m \mathbf{u}_b^T (\mathbf{N}^T \mathbf{p}_m) \tag{35}$$

where t_e and t_k are the thickness of the block e and the interface k , respectively. The stationarity of the modified functional Π^* leads to the following static equilibrium equation for the block–interface system:

$$\mathbf{K}\mathbf{U} = \mathbf{P} \tag{36}$$

where

$$\mathbf{K} = \sum_e t_e \iint_{\Omega_e} \mathbf{B}_b^T \mathbf{D}_b \mathbf{B}_b \, dx \, dy + \sum_k t_k \int_{\beta_k} \mathbf{B}_s^T \mathbf{D}_s \mathbf{B}_s \, ds \quad (37)$$

$$\mathbf{P} = \sum_e \iint_{\Omega_e} \mathbf{N}^T \mathbf{f}_e \, dx \, dy + \sum_m \mathbf{N}^T \mathbf{p}_m \quad (38)$$

$$\mathbf{U} = [u_1, v_1, u_2, v_2, \dots, u_N, v_N]^T \quad (39)$$

and N is the total number of points in the system. In the above equations, \sum presents matrix assembling.

5. ESSENTIAL BOUNDARY CONDITION

Unlike the finite element method, the nodal value of the interpolation function $u^h(\mathbf{x})$ at each point \mathbf{x} is not equal to the nodal value of the function $u(\mathbf{x})$ at the point \mathbf{x} unless the weighting functions are singular, namely

$$\Phi_I(\mathbf{x}_J) \neq \delta_{IJ} \quad (40)$$

consequently, the essential boundary condition should be imposed by Lagrange multipliers or penalty method. The essential boundary condition is

$$\mathbf{u} = \bar{\mathbf{u}} \quad \text{on } \Gamma_u \quad (41)$$

where Γ_u is the prescribed displacement boundary, $\bar{\mathbf{u}}$ is the prescribed displacement vector on boundary Γ_u . To impose the essential boundary condition by Lagrange multipliers, constraint (41) should be removed by adding a Lagrangian term,

$$\Pi_L = - \int_{\Gamma_u} \lambda^T (\mathbf{u} - \bar{\mathbf{u}}) \, d\Gamma \quad (42)$$

in functional (31). Actually, the Lagrange multiplier λ in (42) represents the traction on the boundary Γ_u , hence (42) can be rewritten as

$$\Pi_L = - \int_{\Gamma_u} \mathbf{u}_b^T \mathbf{B}_b^T \mathbf{D}_b^T \mathbf{T}^T (\mathbf{N} \mathbf{u}_b - \bar{\mathbf{u}}) \, d\Gamma \quad (43)$$

where

$$\mathbf{T} = \begin{bmatrix} n_x & 0 & n_y \\ 0 & n_y & n_x \end{bmatrix}$$

and n_x, n_y are the direction cosines of the outward normal to the prescribed displacement boundary Γ_u . The contribution of Π_L to the global stiffness matrix and load vector is given by

$$\mathbf{K}_L = - \int_{\Gamma_u} \mathbf{B}_b^T \mathbf{D}_b^T \mathbf{T}^T \mathbf{N} \, d\Gamma - \int_{\Gamma_u} \mathbf{N}^T \mathbf{T} \mathbf{D}_b \mathbf{B}_b \, d\Gamma \quad (44)$$

$$\mathbf{P}_L = - \int_{\Gamma_u} \mathbf{B}_b^T \mathbf{D}_b^T \mathbf{T}^T \bar{\mathbf{u}} \, d\Gamma \quad (45)$$

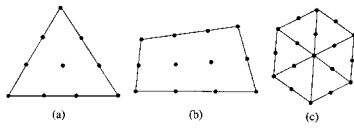


Figure 6. Distribution of points: (a) in a triangle block ($l=3$); (b) in a quadrilateral block ($l=3$, $m=4$) and (c) in a polygon block ($l=2, k=6$).

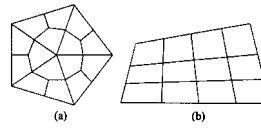


Figure 7. Integration scheme: (a) an arbitrary polygon block ($l=1$); and (b) a quadrilateral block ($l=3, m=4$).

Adding \mathbf{K}_L to the right-hand side of (37) and \mathbf{P}_L to the right-hand side of (38) results in the global equilibrium equation of the system. If the penalty method is used to impose the essential boundary condition, the penalty term,

$$\Pi_a = \frac{\alpha}{2} \int_{\Gamma_u} (\mathbf{u} - \bar{\mathbf{u}})^T (\mathbf{u} - \bar{\mathbf{u}}) d\Gamma \tag{46}$$

where α is the penalty, should be added in functional (31). The contribution of Π_a to the global stiffness matrix and load vector is given by

$$\mathbf{K}_a = \alpha \int_{\Gamma_u} \mathbf{N}^T \mathbf{N} d\Gamma \tag{47}$$

$$\mathbf{P}_a = \alpha \int_{\Gamma_u} \mathbf{N}^T \bar{\mathbf{u}} d\Gamma \tag{48}$$

6. DISTRIBUTION OF POINTS IN BLOCKS

In the present method, displacement fields in blocks are constructed by the moving least-squares interpolants with an array of points. More points should be distributed in the blocks with deep stress gradient than in the others to achieve high accuracy. In this paper, points are distributed automatically according to the following rules:

- (i) For a triangle block, $l + 1$ layers of points are distributed so that there is one point in the first layer, two points in the second layer, three points in the third layer, and so on. Total number of points distributed in the block is $(l + 1)(l + 2)/2$ (see Figure 6(a)).
- (ii) For a quadrilateral block, there are lm points distributed in the block, where l is the number of points distributed on the first and third sides of the block, while m is the number of points allocated on the second and fourth sides (see Figure 6(b)).
- (iii) For an arbitrary polygon block with k sides, it is first divided into k triangles by connecting the centroid of the block and its k vertexes, and then put points in these k triangles according to rule 1. There are $kl(l + 1)/2 + 1$ points distributed in the arbitrary polygon block with k sides (see Figure 6(c)).

7. INTEGRATION SCHEME

Unlike the finite element method, no mesh exists in the present method, hence extra treatment is required in the calculation of integrals in (37) and (38). In order to obtain the integrals, a cell structure, which is independent of the points and arranged in a regular pattern in both dimensions, is used in [7]. In each cell, Gauss quadrature is used. In this method, if a quadrature point is outside the physical domain, the contributions of the quadrature point to (37) and (38) are simply neglected.

In this paper, a block is automatically divided into a number of subdomains according to accuracy requirement, and Gauss quadrature is used in each subdomain. For a triangle block, it is divided into three quadrilateral subdomains by connecting its centroid and the midpoints of its three sides. If it is required, each quadrilateral subdomain could be further divided into four quadrilateral subdomains. For an arbitrary polygon block with k ($k > 4$) sides, it is first divided into k triangle blocks by connecting its centroid and its k vertexes, and then these k triangle blocks are divided into a number of quadrilateral subdomains according to the aforementioned method. There are $3k4^{l-1}$ quadrilateral subdomains obtained (see Figure 7(a)).

For a quadrilateral block, it is divided into lm quadrilateral subdomains, where l is the number of divisions on the first and third sides, and m is the number of divisions on the second and fourth sides (see Figure 7(b)).

Because all blocks are divided into subdomains, all interfaces are also automatically divided into a number of subinterfaces. Gauss quadrature is used in every subinterface.

After dividing all blocks and interfaces into subdomains and subinterfaces, Equations (37) and (38) can be rewritten as

$$\mathbf{K} = \sum_e t_e \sum_i \int_{-1}^1 \int_{-1}^1 \mathbf{B}_b^T \mathbf{D}_b \mathbf{B}_b |\mathbf{J}| d\xi d\eta + \sum_k t_k \sum_i \frac{L_i}{2} \int_{-1}^1 \mathbf{B}_s^T \mathbf{D}_s \mathbf{B}_s d\xi \quad (49)$$

$$\mathbf{P} = \sum_e \sum_i \int_{-1}^1 \int_{-1}^1 \mathbf{N}^T \mathbf{f}_e |\mathbf{J}| d\xi d\eta + \sum_m \mathbf{N}^T \mathbf{p}_m \quad (50)$$

where $|\mathbf{J}|$ is Jacobi determinant, L_i is the length of subinterface i of interface k . The integrals in (49) and (50) can be evaluated by Gauss quadrature.

8. NUMERICAL EXAMPLES

8.1. A jointed rock mass

Singh proposed an equivalent anisotropic elastic model [13] for jointed rock masses which had given excellent results, except in the region of steep stress gradients near the loaded area. The jointed rock mass shown in Figure 8 is analysed for the plane strain case by using the present method. The tangential and normal stiffnesses of the vertical joints are 438.8 and 395.9 GPa/m, respectively; while those of the horizontal joints are 438.8 and 531.9 GPa/m. The elastic modulus of the rock blocks is 89 GPa/m and the Poisson's ratio $\nu_r = 0.26$. According to the theory given by Singh [13], the equivalent anisotropic material properties of the rock mass are obtained as $E_1 = 52.55$ GPa/m, $E_2 = 41.9$ GPa/m and Poisson's ratios $\nu_1 = 0.1535$, $\nu_2 = 0.1224$.

The anisotropic continuum model proposed by Singh is ideally suited to this problem, because the size of the loaded area is quite large compared to the size of the blocks. The mean strain

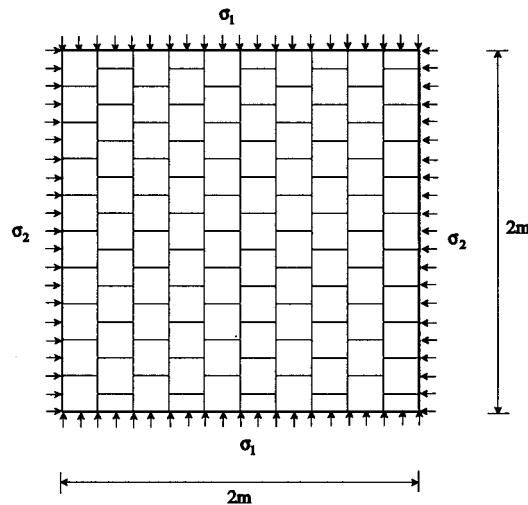


Figure 8. A jointed rock mass.

values of the jointed rock mass obtained by the present method are in excellent agreement with those given by Singh's theory; the maximum error in mean strain is less than 0.5 Per cent. Due to the discontinuities of the jointed rock mass, the displacement fields obtained by the present method are totally different from those obtained by Singh's theory. Compared with Singh's theory, the discontinuities of the rock mass are explicitly taken into account in the present method.

8.2. A semi-infinite jointed rock mass subjected to strip load

The semi-infinite jointed rock mass subjected to strip load shown in Figure 9 is studied. The spacing of the joints is assumed to be $S_2 = 10$ m, the normal and shear stiffnesses of the joints are $K_n = K_s = 0.555$ GPa/m. The rock material is assumed to be isotropic with an elastic modulus $E_r = 50$ GPa, and Poisson's ratio $\nu_r = 0.20$.

This problem is of special interest. Firstly, the strip width is small in comparison with the joint spacing, hence the rock layers will be subjected to a high stress gradient. Further, each layer will behave as a beam, but the bending stresses cannot be taken into account in an anisotropic continuum model. Consequently, an anisotropic continuum model will result in a significant error in the region of steep stress gradients near the loaded area. If a mesh based method is used, the mesh should be sufficiently fine to simulate a high stress gradient in each rock layer.

In the present method, each rock layer is modelled by one block in which 25×5 points are automatically distributed to construct the displacement field. The space integration is performed by using 10 zones in the horizontal direction and three zones in the vertical direction in each rock layer. 3×3 Gauss quadrature is used in each zone to evaluate the stiffness matrix.

To verify the results obtained by the present method, the semi-infinite rock mass is also analysed by using the block-interfaces model [5]. In this analysis, each rock layer is divided into 92 blocks which are connected by interfaces with a very large stiffness to enforce the continuity in the rock layer. The dimensionless vertical deflection, $E_r U / S_2 p$, at the left upper corner obtained by the

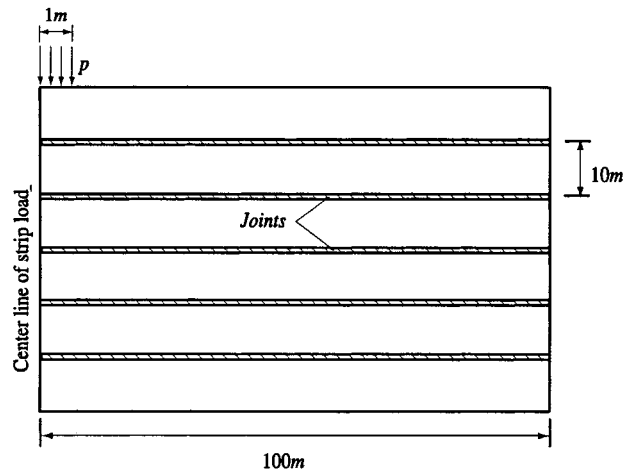


Figure 9. A semi-infinite jointed rock mass subjected to a strip load.

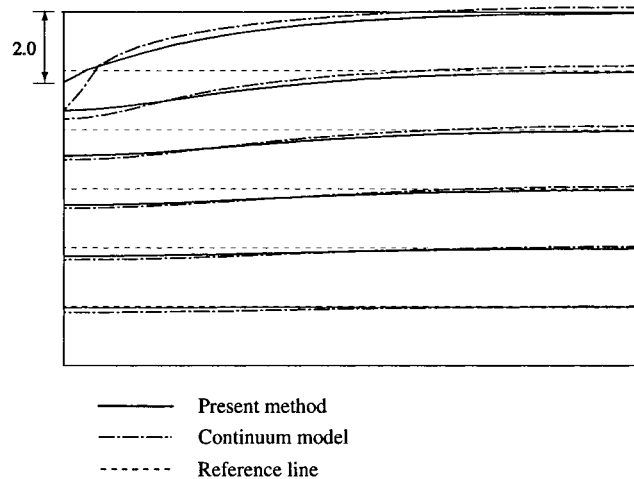


Figure 10. Comparison of the dimensionless vertical deflections computed by the present method and a standard finite element analysis using the anisotropic continuum model proposed by Singh [13].

present method is 1.987, while that obtained by the block–interfaces model is 2.004. They are in excellent agreement.

To study the difference between the present method and an anisotropic continuum model, the semi-infinite rock mass is analysed again by using the standard finite element method with an anisotropic material, whose properties are given by Singh’s theory as $E_1 = 50$ GPa, $E_2 = 5$ GPa, $\nu_1 = 0.2$, $\nu_2 = 0.02$, and $G_{12} = 4.3825$ GPa. The dimensionless vertical deflections, $E_r U/S_2 p$, of the rock mass obtained by the present method and the anisotropic continuum model are compared in Figure 10. It shows that the anisotropic continuum model gives good results for jointed rock

mass, except in the region of steep stress gradient near the loaded area. Based on this study, a large scale jointed rock structure can be analysed efficiently by considering the major part of the structure, in which the stress gradients are moderately low, as anisotropic continuum modelled by a few meshless blocks.

9. CONCLUDING REMARKS

Based on the moving least-squares interpolants, a meshless model is proposed in this paper for the mechanics analysis of jointed rock structures. In this model, no finite element mesh is required and only a number of points are distributed in each block to construct the displacement field, consequently, the time-consuming mesh generation is avoided. The displacement field and its gradients are continuous in each block, hence no post processing is required for the output of strains and stresses. The rate of convergence can exceed that of finite elements significantly and a high resolution of localized steep gradients can be achieved. Furthermore, the discontinuities of rock structures are fully taken into consideration. The present model can be used in the mechanics analysis of complex rock structures, and can be extended to three-dimensional and non-linear analysis.

ACKNOWLEDGEMENTS

This work was supported by the National Natural Science Foundation of China under grant number 59509002.

REFERENCES

1. Goodman RE, Taylor RL, Brekke TL. A model for the mechanics of jointed rock. *ASCE Journal of the Soil Mechanics and Foundation Division* 1968; **94**(SM3):637–659.
2. Cundall PA. A computer model for simulating progressive large scale movements in blocky rock system. *Proceedings of Symposium on Rock Fracture (ISRM)* Nancy, 1971.
3. Shi GH, Goodman RE. Discontinuous deformation analysis. *Proceedings of 25th U.S. Symposium on Rock Mechanics* 1984; 269–277.
4. Qian LX, Zhang X. Rigid finite element method and its applications in engineering. *Acta Mechanica Sinica* 1995; **11**(1):44–50 (English edition).
5. Zhang X, Lu MW. Block-interfaces model for nonlinear numerical simulations of rock structures. *International Journal of Rock Mechanics and Mining Sciences* 1998; **35**(7):983–990.
6. Noh WF. CEL: A time-dependent two-space-dimensional coupled Eulerian-Lagrangian code. In *Methods in Computational Physics*, vol. 3, Alder B, Fernbach S, Rotenberg M (eds). Academic Press: New York, 1964.
7. Belytschko T, Lu YY, Gu L. Element-free Galerkin method. *International Journal for Numerical Methods in Engineering* 1994; **37**:229–256.
8. Liu WK, Chen *et al.* Y. Overview and applications of the reproducing kernel particle methods. *Archive of Computational Methods in Engineering, State of the Art Reviews* 1996; **3**:3–80.
9. Lucy LB. A numerical approach to the testing of the fission hypothesis. *The Astronomical Journal* 1977; **8**(12): 1013–1024.
10. Smart D. Strength of weathered rock. *International Journal of Rock Mechanics and Mining Sciences* 1970; **7**: 371–383.
11. Salamon MDG. Elastic moduli of a stratified rock mass. *International Journal of Rock Mechanics and Mining Sciences* 1968; **5**:519–527.
12. Gerrard CM. Elastic models of rock masses having one, two, three sets of joints. *International Journal of Rock Mechanics and Mining Sciences and Geomechanics Abstracts* 1982; **19**(1):15–23.
13. Singh B. Continuum characterization of jointed rock masses, part I—The constitutive equations. *International Journal of Rock Mechanics and Mining Sciences and Geomechanics Abstracts* 1973; **10**:311–335.
14. Zhang X. Block-seams model for discontinuum mechanics analysis. *Acta Mechanica Sinica* 1997; **29**(3):323–331 (Chinese edition).